Eddy-Current Sensing Principle in Inertial Sensors

Vogel, Johan G.; Chaturvedi, Vikram; Nihtianov, Stoyan

DOI
10.1109/LSENS.2017.2737940

Publication date
2017

Document Version
Final published version

Published in
IEEE Sensors Letters

IEEE Sensors Letters Volume 2(3) (2017)
Inertial sensor

Eddy-Current Sensing Principle in Inertial Sensors

Johan G. Vogel*, Vikram Chaturvedi*, and Stoyan Nihtianov**
Delft University of Technology, Delft, The Netherlands
** Member, IEEE*
*** Senior Member, IEEE*

Received #, current version August 2017.

Abstract— The eddy-current displacement sensing principle is, to the best of our knowledge, not yet used in inertial sensors. The main reasons for this are the important performance limitations of the existing eddy-current sensor solutions, such as: low sensitivity, poor stability, high power consumption and bulkiness. Our novel high-frequency Eddy-Current Displacement Sensor (ECDS), however, has significantly improved performance with respect to these limitations and allows the use of planar, stable coils, making it a viable candidate for use in inertial sensors. An implementation example of an ECDS-based inertial sensor with a bandwidth of 370 Hz and a noise floor of 13 $^{\mu g}/_{\sqrt{Hz}}$ is proposed. Although not yet competitive with state-of-the-art inertial sensors, it performs better than other types of inductive accelerometers and offers the inherent advantages of ECDSs, such as insensitivity to the environment.

Index Terms— Eddy-current sensing, inertial sensor, high-resolution, thermal sensitivity

I. INTRODUCTION

The majority of inertial sensors make use of mass-spring systems whose movement is a measure of acceleration. Strain in the spring structures is often measured using piezoelectric elements [1]; the displacement of the proof mass is commonly sensed by using capacitive electrodes [2]. Deformation may also be sensed by monitoring the inductance of the deforming structure. Examples include a bond-wire accelerometer [3] and a MEMS structure whose suspension springs are used as inductors [4].

The displacement of the proof mass could also be measured with an Eddy-Current Displacement Sensor (ECDS). An ECDS typically consists of a coil whose inductance varies as a function of the distance from a conductive target. ECDSs offer several advantages over capacitive displacement sensors: they are insensitive to environmental conditions such as pressure, humidity and contamination and their operation is fully contactless, as no electric grounding of the target is required [5, 6].

At the same time, state-of-the-art ECDSs are, to the best of our knowledge, not used in inertial sensors as they have several limitations. They are relatively bulky owing to their external readout electronics. Some major limitations are caused by their low excitation frequencies (~1-2 MHz). The measurement of the ECDSs not only depends on the target distance, but also on the skin-depth δ, i.e. the depth at which the eddy-current intensity in the target reduces to 37 %. The skin-depth depends on the excitation frequency f_{exc} and the conductivity of the target, which is sensitive to temperature. As δ limits the displacement sensitivity and leads to high sensitivity to temperature, it should be minimised by employing a higher excitation frequency [6].

A novel ECDS solution has been proposed that mitigates the negative aspects of the ECDS while preserving the advantages by: (i) increasing the excitation frequency in the range of hundreds of MHz to mitigate limitations related to the skin effect; (ii) using a small flat sensing coil for mechanical stability and compactness; (iii) using a self-oscillating operating mode in the readout electronics to reduce the power consumption [6, 7]; (iv) implementing a ratiometric readout to improve mechanical and thermal stability [11].

This letter describes the architecture of this novel ECDS and its potential to be used in inertial sensing applications, by presenting an example of an accelerometer design and comparing its noise performance/resolution with the state-of-the-art.

Corresponding author: J. G. Vogel (j.g.vogel@tudelft.nl).
Digital Object Identifier: 10.1109/LSEN.XXXX.XXXXXXX (inserted by IEEE).

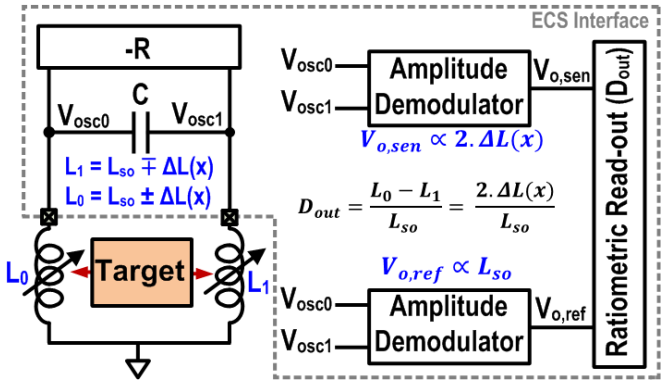

Fig. 1. Architecture of the eddy-current sensor solution. The resonator (left) consists of the two coils and an on-chip capacitor.

II. EDDY-CURRENT SENSOR SOLUTION

A. Architecture

The ECDS solution consists of two coils and a readout interface. The interface excites the coils with a high-frequency current, generating a magnetic field that induces eddy-currents in a nearby conductive target. The secondary magnetic field created by the eddy-currents causes a change in the inductance of the coils, which depends on the relative displacement between the coils and the target. If the coils are placed at opposite sides of the target, their inductance changes in the opposite direction, making a differential measurement possible.

Fig. 1 shows the architecture of the ECDS solution. The coils, together with an on-chip capacitor C, form an LC oscillator. The output voltages of the oscillator V_{osc0} and V_{osc1} are proportional to the coil inductances L_0 and L_1, respectively. After demodulation, the ratio D_{out} between the amplitudes of V_{osc0} and V_{osc1} is used as the measure of the displacement of the target.

Three of the design choices play important roles in the performance of the ECDS interface: (i) the oscillation amplitude acts as the information carrier for the position of the target; (ii) synchronous amplitude demodulation is used; (iii) ratiometric measurement suppresses correlated-multiplicative errors such as gain drift [8]. In the case of a single-ended measurement, the excitation frequency of the oscillator can also be used as a measure of the inductance, instead of the oscillation amplitude [3, 4]. However, the oscillation amplitudes V_{osc0} and V_{osc1} were chosen because of their higher sensitivity to inductance change. Furthermore, synchronous amplitude demodulation allows high resolution to be attained with moderate power dissipation [8].

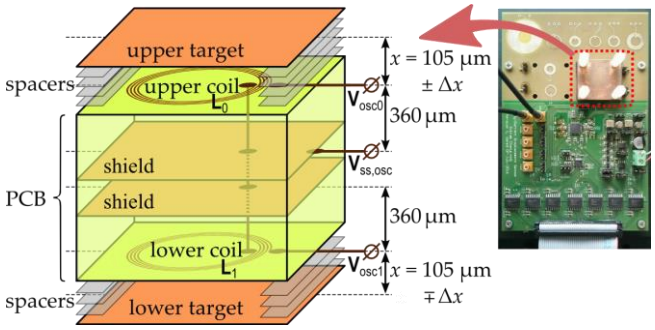

Fig. 2. Cross-section of the four-layer PCB and the targets that were fixed using stainless steel spacers.

B. Benefits for Inertial Sensors

High-performance industrial eddy-current sensors typically use external electronics with significant power consumption (tenths of watts to several watts). The power consumption of the integrated ECDS interface is relatively low (~20 mW), making it possible to integrate the electronics into the sensor probe [11]. This allows the parasitic cable inductance to be eliminated, so that relatively low-inductance planar coils can be used, which have higher mechanical stability than wound coils. Moreover, the use of planar coils and integrated readout electronics allow for compact sensor design, which is a necessary requirement in inertial sensing.

The excitation frequency of the interface is around 126 MHz, much higher than the off-the-shelf ECDSs, which operate at 1-2 MHz. By using a high excitation frequency in combination with a low standoff (~100 µm), it is possible to obtain high displacement sensitivity. At the increased excitation frequency, the skin depth reduces, allowing measurement with respect of thin membranes (thickness > 20 µm) without a loss of sensitivity or added instability. The reduced skin-depth also lowers the sensitivity to the temperature of the target by approx. a factor of 10. The sensitivity to thermal expansion of the sensor's geometry is reduced by measuring differentially with respect to a single target [9, 10].

C. Experimental Setup

The performance of the eddy-current displacement sensor was assessed using a customized PCB prototype. In our earlier work [11], this prototype was used to determine the noise floor of the interface and the sensor characteristic of a single-ended displacement sensor. Here the prototype is used to obtain the sensor's differential transfer characteristic, which is relevant for

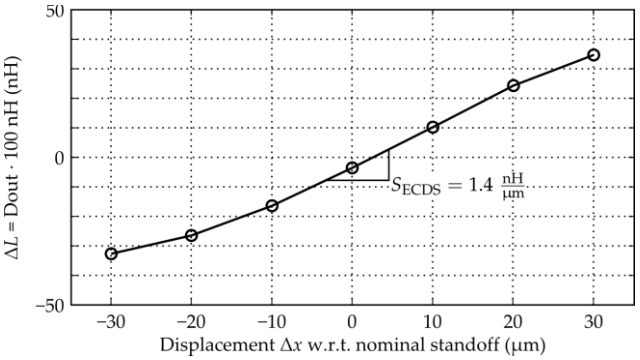

Fig. 3. Measured transfer characteristic of the differential ECDS.

inertial sensing application.

Fig. 2 shows the cross-section of the four-layered PCB. The upper and lower copper layers contain the coils (8 mm diameter, 4 turns, 0.2 mm pitch, 100 nH inductance); two intermediate layers shield the coils from each other. Using 10-µm thick stainless steel spacers, placed >1 mm from the coil, copper targets were positioned at various standoff distances around a nominal standoff of 105 µm.

D. Performance

Fig. 3 shows the sensor's transfer characteristic that was obtained by measuring the sensor's output at various standoffs. Around its nominal standoff, the inductance sensitivity of the sensor is $S_{ECDS} = 1.4\ ^{nH}/_{\mu m}$. Further away from the nominal standoff, the transfer characteristic saturates due to the limited output voltage range of the electronics. The measured noise level of the interface was found to be $13\ ^{fH}/_{\sqrt{Hz}}$ [11], which is equivalent to $9.3\ ^{pm}/_{\sqrt{Hz}}$ noise in terms of differential displacement.

III. IMPLEMENTATION IN AN INERTIAL SENSOR

Many inertial sensor designs are presented in the literature. Some of them use surface micromachining, and others bulk micromachining [12]. In [13] a single-ended inductive accelerometer design is presented that is based on bulk micromachining. The geometry choices lead to a certain mechanical eigenfrequency ω_0, which directly determines the mechanical sensitivity:

$$S_{\text{mech}} = \frac{\Delta x}{a} = \frac{1}{\omega_0^2}.$$

As the sensor's bandwidth is limited by the eigenfrequency, there is an inherent trade-off between mechanical sensitivity and bandwidth.

Fig. 4 shows an implementation example of the eddy-current accelerometer based on the design of [13]. Here, the proof mass contains copper surfaces that function as

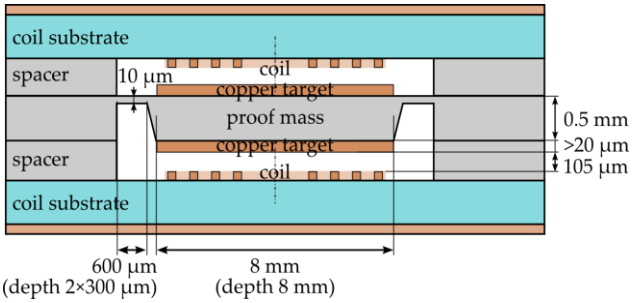

Fig. 4. Implementation example of an inertial sensor that uses eddy-current sensing to determine the displacement of the proof mass.

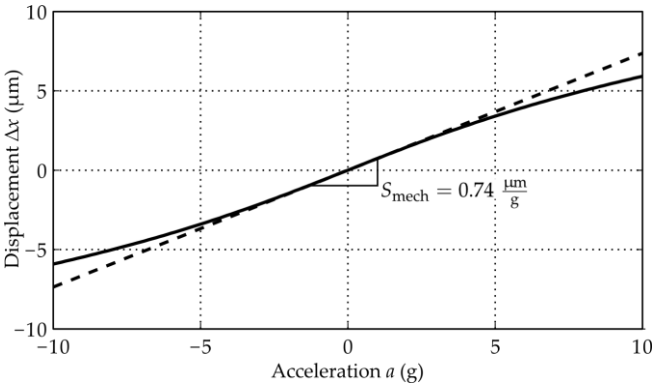

Fig. 5. Simulated mechanical sensitivity of the inertial sensor design.

targets for the eddy-current coils and is suspended from both sides by thin cantilever beams.

The inertial sensor is modelled using finite elements in Comsol. It has an eigenfrequency of around 580 Hz and a mechanical sensitivity of $S_{\text{mech}} = 0.74\ ^{\mu m}/_{g}$. In combination with the noise specification of $9.3\ ^{pm}/_{\sqrt{Hz}}$, this leads to an expected acceleration noise floor NF_a of $13\ ^{\mu g}/_{\sqrt{Hz}}$. Assuming the system is critically damped, which is a desirable property for accelerometers [14], the −3 dB bandwidth is $BW \approx 0.64\omega_0 = 370$ Hz.

The range of the inertial sensor (approx. ±10 µm, Fig. 3) is not limited by the linearity of the ECDS, but by the linear range of the design example. An allowed maximum non-linearity error of 6 % corresponds to a deflection of ±3 µm (Fig. 5) and an acceleration range a_{range} of ±4 g (20 % corresponds to ±6 µm and ±10 g). The limited range is caused by the spring stiffening of the double-sided suspension.

Table 1 compares the proposed ECDS solution to state-of-the-art accelerometers of various types. The relative sensitivity S_{rel} of the ECDS is significantly better than the sensitivity of the inductance-based sensor in [3] and comparable to the one in [4].

In Table 1 two accelerometer Figure of Merits (FOMs) are used from the literature [16, 17], i.e.:

Table 1. Comparison of the proposed ECDS and state-of-the-art capacitive (Cap.), silicon oscillating (SOA) and inductive (Ind.) accelerometers. *DR* is dynamic range.

	[15]	[16]	[17]	[18]	[3]	[4]	This work
Type	Cap.	Cap.	Cap.	SOA	Ind.	Ind.	ECDS
P (mW)	12	3.6	23	3.5	9	-	19.8
BW (kHz)	0.30	0.20	0.30	0.20	5	<2.0	0.37
NF_a ($^{\mu g}/_{\sqrt{Hz}}$)	1.15	2.0	0.20	2.0	700	-	13
$S_{rel} \cdot 10^{-3}$ ($^{(si/si)}/_{g}$)	-	420	56	-	0.008	4.3	10
a_{range} (g)	±11	±1.2	±1.2	±20	±3.0	-	±4
DR (dB)	115	92	111	117	36	-	84
FOM_1 ($^{nW}/_{Hz}$)	0.072	0.44	0.22	0.025	30	-	3.3
FOM_2 ($^{nW \cdot g}/_{Hz}$)	0.80	0.51	0.27	0.49	89	-	13

$$FOM_1 = \frac{P}{\sqrt{BW}} \frac{NF_a}{a_{\text{range}}} \quad \text{and} \quad FOM_2 = \frac{P \cdot NF_a}{\sqrt{BW}}.$$

The performance of the presented ECDS-based inertial sensor is much better than the inductance-based sensor in [3], but not yet competitive with the other state-of-the-art inertial sensors in the table. The main reason is that the presented implementation example is based on the ECDS design proposed in [11], which has significant room for further optimisation. It is possible to reduce the nominal standoff to improve sensitivity S_{ECDS}. Furthermore, the power consumption of the interface can be optimised for differential operation, leading to a reduction of approx. 50 %. The dimensions of the coils can be reduced to a diameter of a few millimetres to decrease the sensor's surface area.

IV. CONCLUSION

The high excitation frequency (126 MHz) and relatively low power consumption (19.8 mW) of our ECDS solution with respect to the state-of-the-art ECDSs enables the use of planar coils and a thin measurement target. Together with a high sensitivity and a moderate noise floor, these advantages make the eddy-current principle a viable candidate for inertial sensing, offering the inherent benefits of the eddy-current principle.

A design example to be fabricated using bulk micromachining can achieve a range of ±4 g and a noise level of 13 $^{\mu g}/_{\sqrt{Hz}}$ for a 370 Hz bandwidth. Although the reported performance is not yet competitive with state-of-the-art accelerometers, it is better than other inductive accelerometers. To improve the performance for inertial sensing, the ECDS needs further optimisation. Our future work will involve optimisation, manufacturing and evaluation of the optimised sensor.

REFERENCES

[1] S. Tadigadapa and K. Mateti, "Piezoelectric MEMS sensors: state-of-the-art and perspectives," Measurement Science and Technology, vol. 20, no. 9, p. 92001, 2009.
[2] C. Acar and A. M. Shkel, "Experimental evaluation and comparative analysis of commercial variable-capacitance MEMS accelerometers," Journal of Micromechanics and Microengineering, vol. 13, no. 5, p. 634, 2003.
[3] Y. T. Liao, S. C. Huang, F. Y. Cheng, and T. H. Tsai, "A Fully-Integrated Wireless Bondwire Accelerometer With Closed-loop Readout Architecture," IEEE Transactions on Circuits and Systems I: Regular Papers, vol. 62, no. 10, pp. 2445–2453, Oct. 2015.
[4] Y. Chiu, H. C. Hong, and C. W. Lin, "Inductive CMOS MEMS accelerometer with integrated variable inductors," in IEEE 29th International Conference on Micro Electro Mechanical Systems, 2016, pp. 974–977.
[5] Fleming, A. A review of nanometer resolution position sensors: Operation and performance Sensors and Actuators A: Physical, vol. 190, pp. 106 – 26, 2013.
[6] S. Nihtianov, "Capacitive and Eddy Current Displacement Sensors: Advantages and Limitations", IEEE Industrial Electronics Magazine (IEM), vol. 8, pp. 6 – 15, March 2014.
[7] M. R. Nabavi, et al., "An interface for eddy-current displacement sensors with 15-bit resolution and 20 MHz excitation," JSSC, vol. 48, pp. 2868 – 81, 2013.
[8] V. Chaturvedi, M. R. Nabavi, J. G. Vogel, and S. Nihtianov, "Demodulation Techniques for Self-Oscillating Eddy-Current Displacement Sensor Interfaces: A Review," IEEE Sensors Journal, 2017.
[9] G. H. Ames, "Thermally balanced differential accelerometer," US2016209439 (A1), 21-Jan-2016.
[10] J. J. Anagnost and A. L. Bullard, "Hung mass accelerometer with differential Eddy current sensing," US2014157897 (A1), 12-Jun-2014.
[11] V. Chaturvedi, M. R. Nabavi, J. G. Vogel, K. A. A. Makinwa, and S. Nihtianov, "A 0.6 nm resolution 19.8mW eddy-current displacement sensor interface with 126MHz excitation," in Proceedings of the ISSCC Í7, 2017.
[12] R. Mukhiya, R. Gopal, B. D. Pant, V. K. Khanna, and T. K. Bhattacharyya, "Design, modeling and FEM-based simulations of a 1-DoF MEMS bulk micromachined piezoresistive accelerometer," Microsystem Technologies, vol. 21, no. 10, pp. 2241–58, 2015.
[13] E. Abbaspour-Sani, R.-S. Huang, and C. Y. Kwok, "A novel electromagnetic accelerometer," IEEE Electron Device Letters, vol. 15, no. 8, pp. 272–273, Aug. 1994.
[14] R. P. van Kampen, M. J. Vellekoop, P. M. Sarro, and R. F. Wolffenbuttel, "Application of electrostatic feedback to critical damping of an integrated silicon capacitive accelerometer," *Sensors and Actuators A: Physical*, vol. 43, no. 1, pp. 100–106, 1994.
[15] M. Pastre *et al.*, "A 300Hz 19b DR capacitive accelerometer based on a versatile front end in a 5th-order ΔΣ loop," *2009 Proceedings of ESSCIRC*, pp. 288–291, Sep. 2009.
[16] M. Yucetas, M. Pulkkinen, A. Kalanti, J. Salomaa, L. Aaltonen, and K. Halonen, "A High-Resolution Accelerometer With Electrostatic Damping and Improved Supply Sensitivity," *IEEE Journal of Solid-State Circuits*, vol. 47, no. 7, pp. 1721–1730, Jul. 2012.
[17] H. Xu, X. Liu, and L. Yin, "A Closed-Loop ΣΔ Interface for a High-Q Micromechanical Capacitive Accelerometer With 200 ng/ surd Hz Input Noise Density," IEEE Journal of Solid-State Circuits, vol. 50, no. 9, pp. 2101–2112, Sep. 2015.
[18] Y. Zhao et al., "A Sub-µg Bias-Instability MEMS Oscillating Accelerometer With an Ultra-Low-Noise Read-Out Circuit in CMOS," IEEE Journal of Solid-State Circuits, vol. 50, no. 9, pp. 2113–2126, Sep. 2015.